

Methods for Autonomous Measurement of 3D Joint Kinematics from 2D Fluoroscopic Images

A Dissertation Defense

Andrew Jensen

March 4, 2024

Outline

Background

Aims

Aim 1 - Joint Track Machine Learning

Aim 2 - Correcting Symmetric Implant Ambiguity

Aim 3 - Musings on a “Kinematics Translator” and Synthetic Kinematics Data

Aim 4 - This will definitely work on shoulders, right?

Conclusion

References

Acknowledgments

I would like to thank the McJunkin Family Charitable Foundation for their generous grant that supports this work.

The Problem

- By 2030, roughly 3.5 million Total Knee Arthroplasty (TKA) will be performed in the US [21].
- 20% of patients receiving TKA are dissatisfied.
 - Instability, pain, unnatural [5, 8, 29].
- No reliable method of clinically assessing and quantifying joint dynamics.
 - Human supervision
 - Time consuming
 - Specialized equipment



Our Proposition

Orthopaedic surgeons and clinicians would readily adopt a **practical** and **inexpensive** technology that allows them to **measure** a patient's knee kinematics during **activities of daily living**.



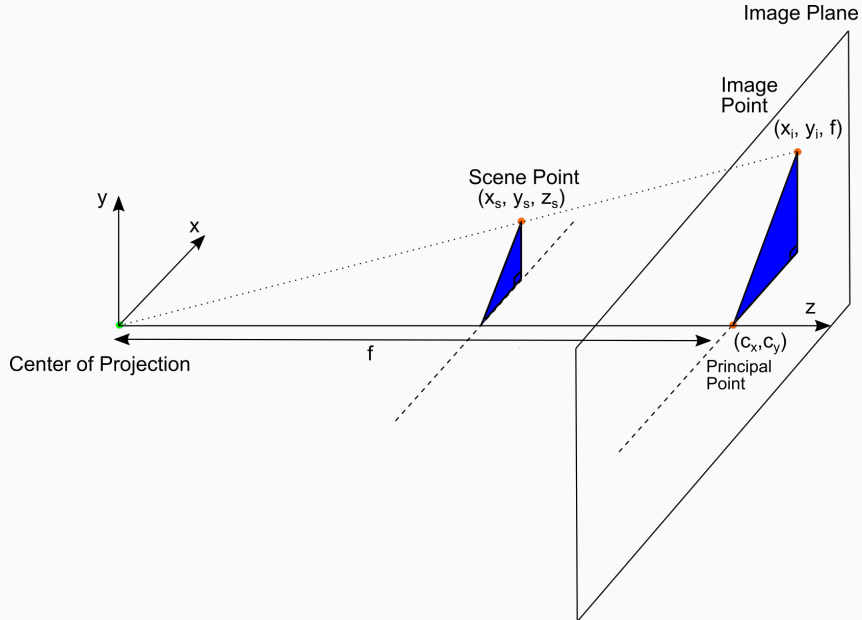
Constraints

- It must fit within a **standard clinical workflow**
- The technology must utilize equipment **commonly found in hospitals**
- There must not be significant **human supervision** nor interaction to generate an examination report.



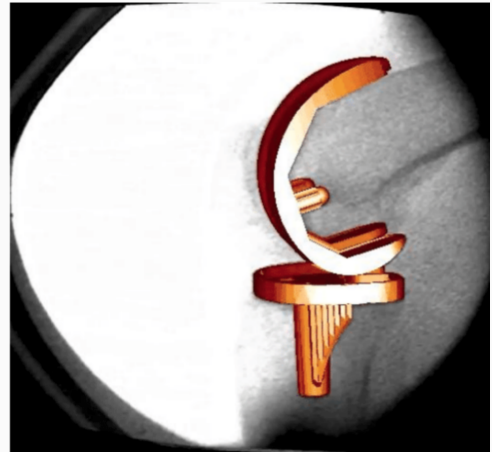
Background

Background - Projective Geometry



Background - Model-Image Registration

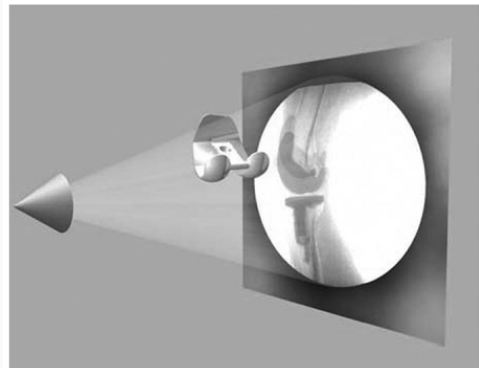
If we know the projective parameters of the fluoroscopy machine, can we tinker with $T_{implant}^{cam}$ so that our virtual projection matches the fluoroscopic image?



From [27]

Background - Model-Image Registration

If we know the projective parameters of the fluoroscopy machine, can we tinker with $T_{implant}^{cam}$ so that our virtual projection matches the fluoroscopic image?



From [27]

Historical Overview

Many different approaches have attempted to solve the model-image registration problem.

- Pre-computed projections
- Skin-mounted motion Capture
- Biplane Imaging
- Iterative Projections
- Roentgen Stereophotogrammetry

Pre-Computed Projections

- Saving space and memory by pre-computing as much as possible.
- Pre-computed distance maps [34, 23].
- Pre-computed shape libraries [6]

From [23]

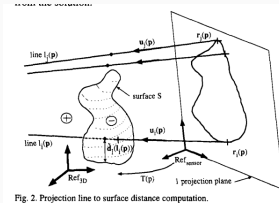
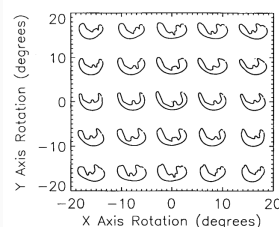


Fig. 2. Projection line to surface distance computation.



From [6]

Limitations of Pre-Computed Projections

- Requires an accurate contour from the input image in order to perform calculations.
 - Human supervision for isolated contour
 - Inaccuracy with naive edge detection

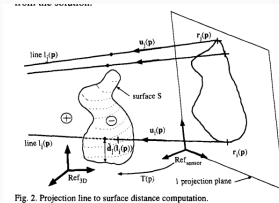
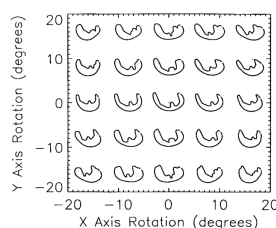


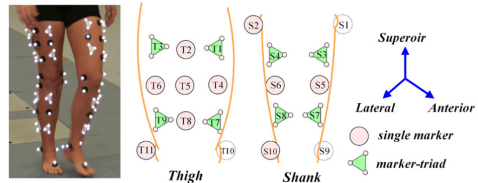
Fig. 2. Projection line to surface distance computation.

From [23]



From [6]

Motion Capture (MoCap)



- Can measure motion of MoCap beads very accurately.
- Skin-mounted [14, 20, 26].
- Bone pins [22].

From [14]

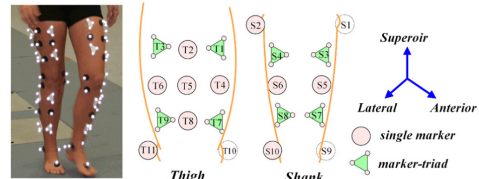


From [22]

Limitations of Motion Capture

Skin Mounted

- Doesn't accurately describe underlying skeletal motion with clinical accuracy [14, 20, 26].



From [14]

Bone Pins

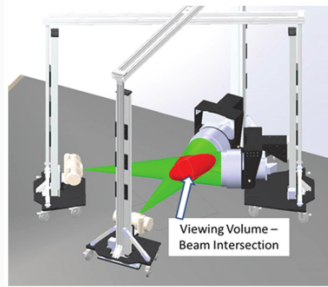
- Any volunteers?



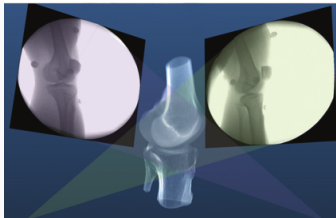
From [22]

Biplane Imaging

- Utilizes multiple cameras to resolve 3D position and orientation[16, 10].
 - Highly accurate.
 - Gold Standard.

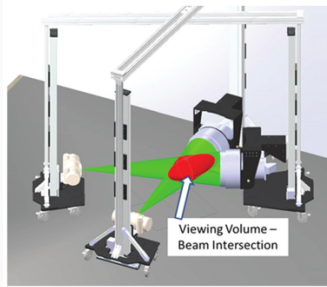


Both from [16]

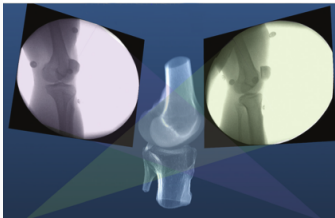


Limitations of Biplane Imaging

- Not many hospitals have biplane fluoroscopy setups.
- Clinically impractical

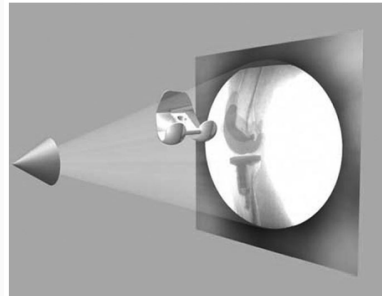


Both from [16]



Iterative Projections

- Take advantage of modern computational graphics pipelines to quickly perform projection matching.
 - Image/Intensity similarity metrics [27]
 - Feature/Contour similarity metrics [13]



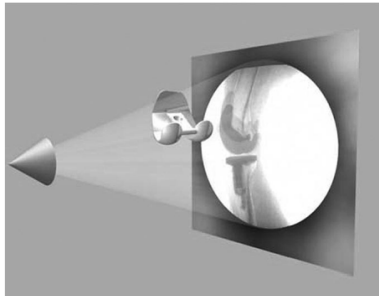
From [27]



From [13]

Limitations of (historic) Iterative Projection Methods

- Requires human supervision for:
 - Pose initialization
 - Escaping local minima
 - Implant detection
- Chaotic and Noisy objective function



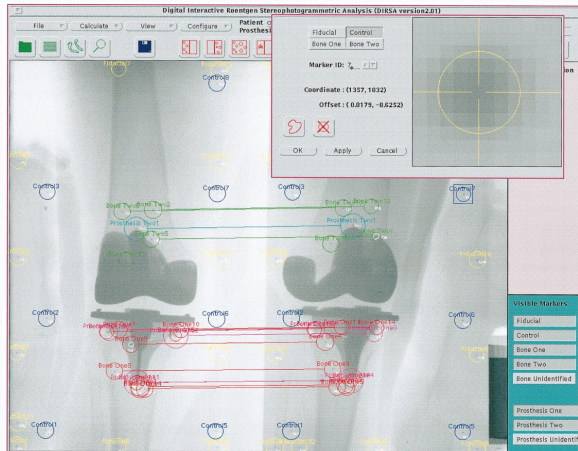
From [27]



From [13]

Roentgen Stereophotogrammetry (RSA)

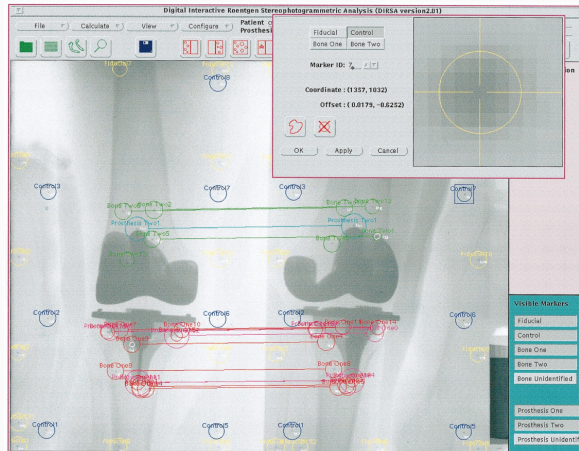
- Uses implanted tantalum beads for motion tracking [32, 30]
- Extremely accurate [19, 28]
- Gold standard Measurement [9]



From [32]

Limitations of RSA

- Involves additional surgical procedures for inserting tantalum beads.
- Human supervision
- Bi-plane imaging



From [32]

Aims

Aims

Aim 1: Joint Track Machine Learning: An Autonomous Method of Measuring Total Knee Arthroplasty Kinematics From Single-Plane X-Ray Images¹

Aim 2: Correcting Symmetric Implant Ambiguity in Measuring Total Knee Arthroplasty Kinematics from Single-Plane Fluoroscopy²

Aim 3: Some Musings on a “Kinematics Translator” and Synthetic Kinematics Data

Aim 4: This will definitely work on shoulders, right?³

¹Published in the Journal of Arthroplasty [18]

²In Revision for Publication in the Journal of Biomechanics

³In Review for Publication in the Journal of Computers in Biology and Medicine

Background

Aims

Aim 1 - Joint Track Machine Learning

Aim 2 - Correcting Symmetric Implant Ambiguity

Aim 3 - Musings on a “Kinematics Translator” and Synthetic Kinematics Data

Aim 4 - This will definitely work on shoulders, right?

Conclusion

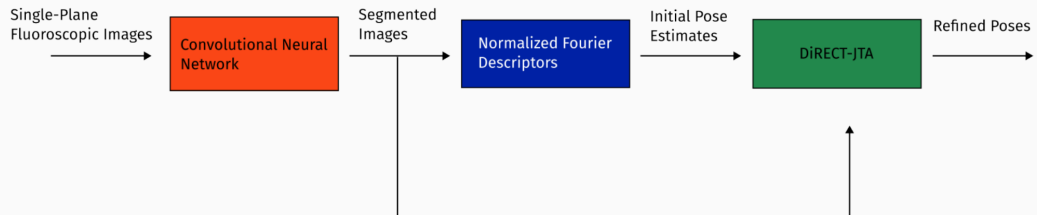
References

Goal

Demonstrate the feasibility of a fully autonomous, model-image registration pipeline.

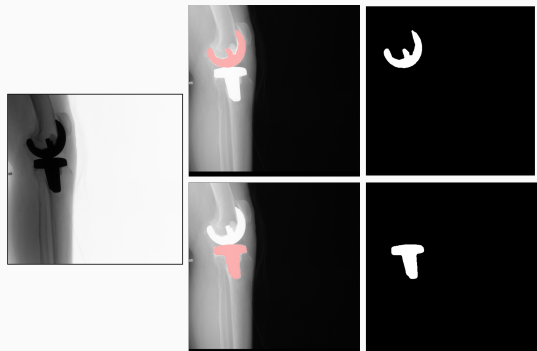
Method

- Three-tiered approach
 - Convolutional Neural networks (CNN) for autonomous implant detection
 - Normalized Fourier Descriptor shape libraries
 - Robust contour-based global optimization scheme



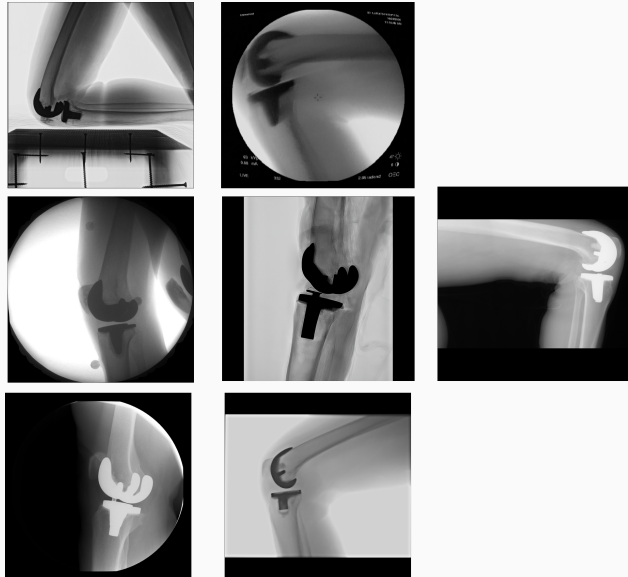
Autonomous Implant Detection Using Convolutional Neural Networks

- 2 CNNs
 - Femoral and Tibial implants
- High Resolution Network [33]



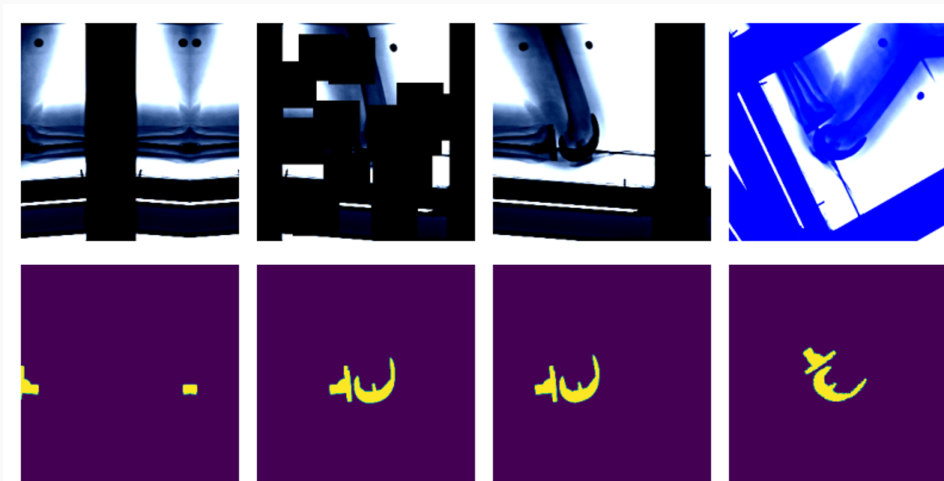
Neural Network Data

- ~8000 images
 - 7 TKA kinematics studies
 - 71 subjects
 - 7 implant manufacturers
 - 36 distinct implants
 - Squat, lunge, knee, stair ascent



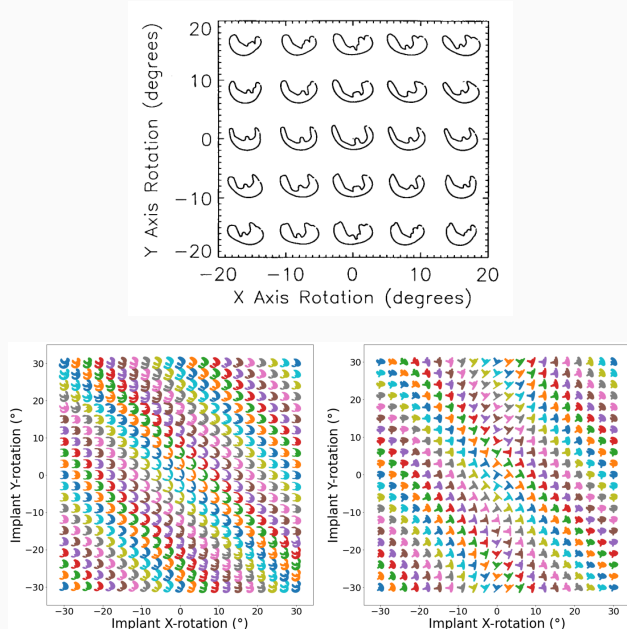
Neural Network Robustness

- Additional augmentations introduced during training [11].



Normalized Fourier Descriptor Shape Libraries

- Pose initialization using segmentation output.
- $\pm 30^\circ$ library span at 3° increments.



Pose Refinement Using Global Optimization

- Two main features
 - Objective function
 - Optimization routine

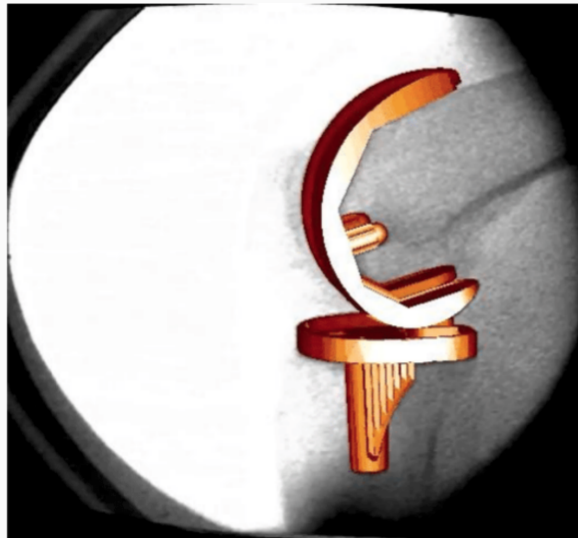
$$\underset{x}{\operatorname{argmin}} \{f(x) : x \in \Omega\}$$

Contour-based Objective Function

- With accurate projection, contours provide a strong heuristic for orientation.
- Overlapping pixels between CNN segmentation and projected implant.
 - L_1 norm has quick parallel computation.

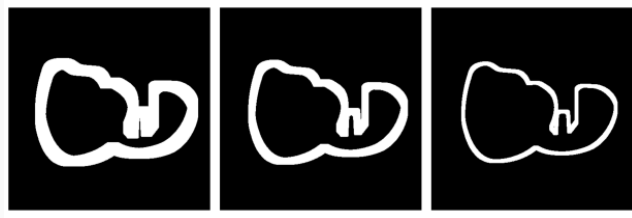
$$J = \sum_{i \in H} \sum_{j \in W} |I_{ij} - P_{ij}| = L_1(I, P)$$

- Sensitive to minor perturbations



Improving Robustness

- Dilation decreases sensitivity to perturbations.
- Multi-stage optimization can reduce dilation back to original edges.

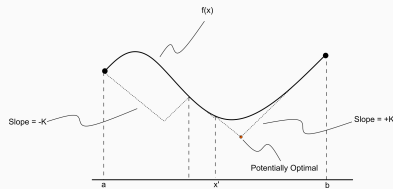
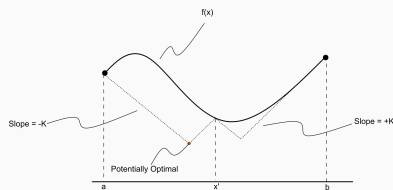
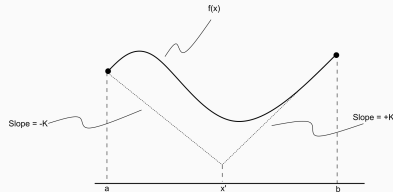


Optimization Routine

- No analytic form of the objective function exists, it **must** be sampled at points of interest.
 - Black Box Optimization [3, 4]

Lipschitzian Optimization

- Robust, global, black-box optimization routine if Lipschitz constant (K) is known [31].
- Lipschitz constant bounds the rate of change of a function.
- What if you don't know the Lipschitz constant?

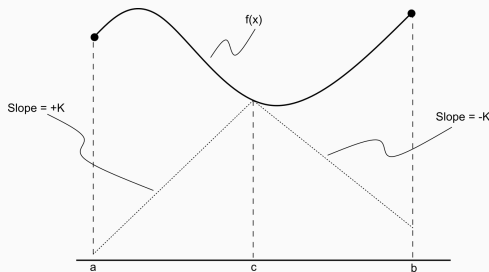


Lipschitzian Optimization without the Lipschitz Constant

Lipschitzian Optimization Without the Lipschitz Constant

D. R. JONES,¹ C. D. PERTTUNEN,² AND B. E. STUCKMAN³

- Sample end-points instead of intersecting lines.
- Potentially optimal regions based on value at center and total size.
 - Trisect potentially optimal regions and re-sample centers



Trisecting Region

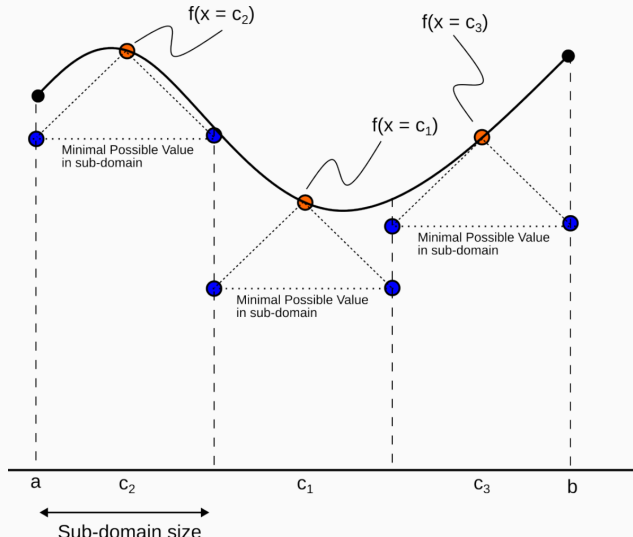
$$\begin{bmatrix} f(x = c_1) & d(c_1) \\ f(x = c_2) & d(c_2) \\ \vdots & \vdots \\ f(x = c_N) & d(c_N) \end{bmatrix}$$

Where

$f(x = c_i) \equiv$ Sampled function value

$d(c_i) \equiv$ Sub-domain size

for $i \in [1, N]$



Another Iteration

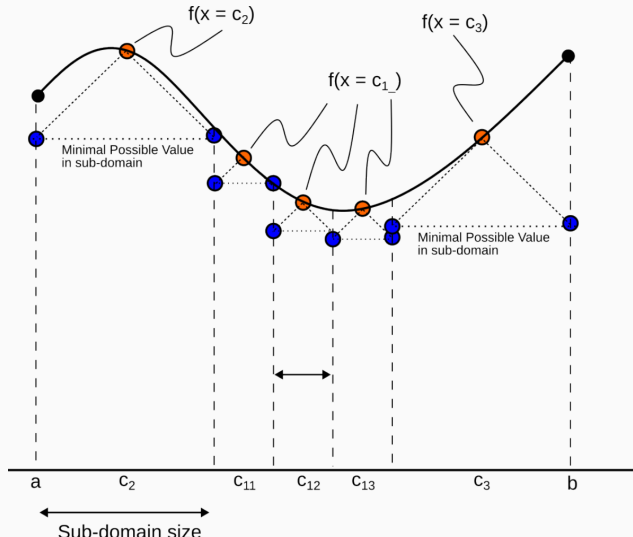
$$\begin{bmatrix} f(x = c_1) & d(c_1) \\ f(x = c_2) & d(c_2) \\ \vdots & \vdots \\ f(x = c_N) & d(c_N) \end{bmatrix}$$

Where

$f(x = c_i) \equiv$ Sampled function value

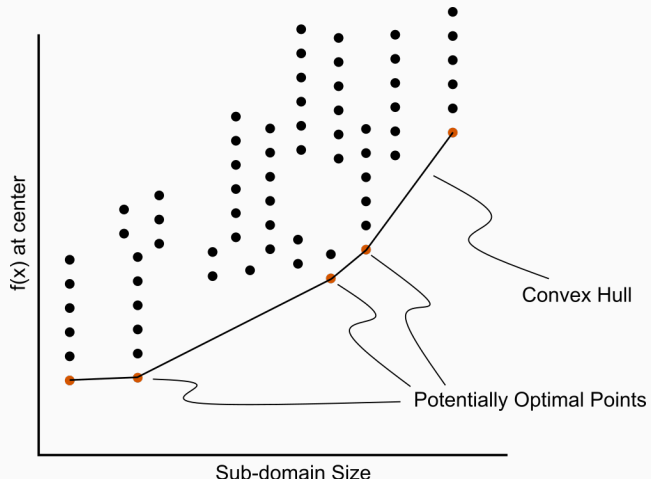
$d(c_i) \equiv$ Sub-domain size

for $i \in [1, N]$



Determining Potentially Optimal Regions

- Convex hull [15, 17, 12, 7] of region size vs. center value



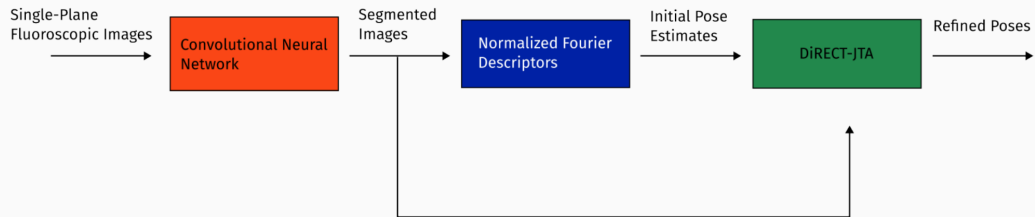
DiRECT for Joint Track Machine Learning

- Search region is along all 6 degrees of freedom.
 - Normalize to $[0, 1]$.
- Three stages, each with decreasing levels of dilation.
 - Iteration budget for each stage.

Stage	Budget [Iterations]	Search Range [mm,deg]	Dilation (pixels)
“Tree”	~20,000	± 45	5
“Branch”	~20,000	± 25	3
“Leaf”	~10,000	± 100 (z_{trans}) / ± 3 (<i>else</i>)	1

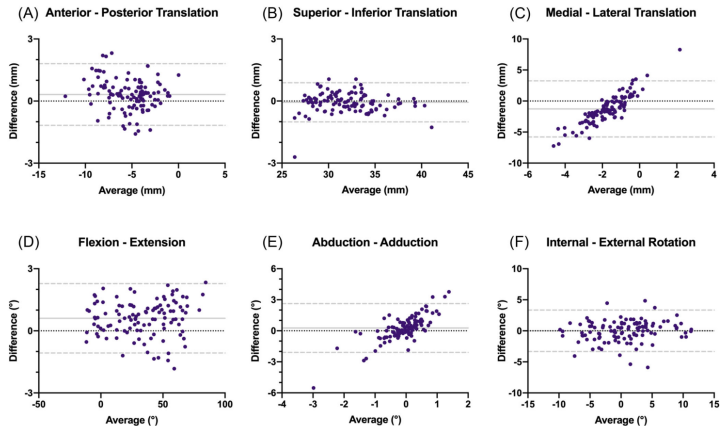
Testing Performance

Now that we have our refined poses, how well does our system perform?



Validation

- Independent research group using Model-Based RSA.
- Determine the level of concordance between the two measurement systems
 - Bland-Altman Plots
- Achieved clinically acceptable accuracy [9, 18].
- Highly repeatable



Awards

The work presented in this aim won the HAP Paul Award for Best Paper from the International Society for Technology in Arthroplasty's 2022 Annual Meeting.



Background

Aims

Aim 1 - Joint Track Machine Learning

Aim 2 - Correcting Symmetric Implant Ambiguity

Aim 3 - Musings on a “Kinematics Translator” and Synthetic Kinematics Data

Aim 4 - This will definitely work on shoulders, right?

Conclusion

References

Goal

- The goal of this aim is to validate and test methods that can overcome single-plane limitations for model-image registration.
 - Out-of-plane (OOP) Translation
 - Symmetry Traps

Translation

- Depth perception is lost when using a single camera.
- Utilize a virtual “spring” to constrain relative OOP translation between implant components.

$$J = \alpha L_1(I, P) + \beta ML(Fem, Tib)$$

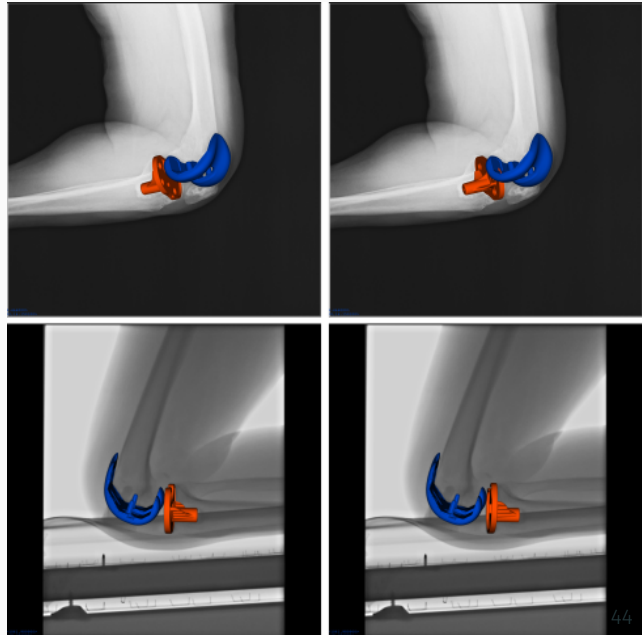
Where

$ML \equiv$ Relative mediolateral translation

Symmetry Traps

With a symmetric tibial implant, the contour is not always a perfect heuristic for true pose.

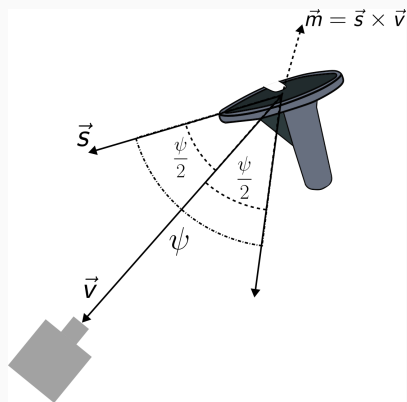
Found “ambiguous zone” within 3° of pure lateral pose with high propensity for symmetry traps [18].



Solving the Symmetric Pose

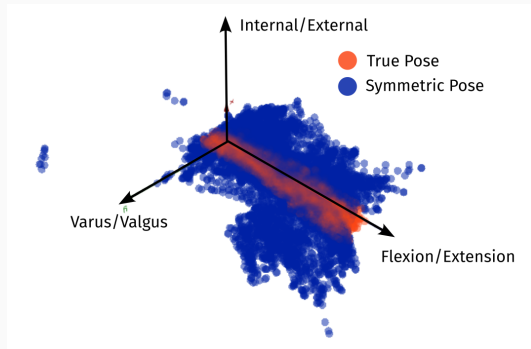
Algorithm devised to “flip” pose into symmetric counterpart.

1. Determine viewing ray from camera to implant centroid, denote \vec{v} , normalize.
2. Denote symmetric-plane normal vector \vec{s} , normalize.
3. Measure relative “off-lateral” orientation of implant, $\cos(\theta) = \frac{\vec{v} \cdot \vec{s}}{||\vec{v}|| ||\vec{s}||}$
4. Apply body-centered rotation to implant about $\vec{m} = \vec{s} \times \vec{v}$ by $\psi = 2\theta$.



Methods - Training Set

- “Symmetric” poses for each of the 12,000 frames were calculated using the “flipper” algorithm, yielding ~24,000 total training samples. The input for each sample was $[\theta_{F/E}, \theta_{V/V}, \theta_{I/E}, \psi]$, and the output was one of {True, Symmetric}



The training data plotted with each axis representing an anatomical rotation (origin not to scale).

Methods - Machine Learning

Using `scikit-learn`, the following classifiers were implemented:

- Support Vector Machine, K-Nearest-Neighbors, AdaBoost, Histogram Gradient Boosting, Bagging Estimator, Stacked Generalization, Majority Voting Classifier

Methods - Fixing “Symmetry Traps”

For an input image sequence, the following is performed:

1. Each pose and its symmetric counterpart are fed into the machine learning classifier
 - 1.1 If the outputs are different, take the pose labeled “true” as the correct pose.
 - 1.2 If the outputs are the same, (i.e. both a pose and its symmetric counterpart return “true”), label image “ambiguous”
2. For all images that are NOT ambiguous, construct a cubic spline through the three rotation measurements.
3. For all images that are labeled “ambiguous”, determine which of the two poses is closer to the spline, and take that as the “correct” pose.

Results - ML Classification

Table 1: Machine Learning Classifier Performance						
Classifier	Tuned Hyperparameters	Test Set	Accuracy (%)	Sensitivity (%)	Specificity (%)	F1-Score
Support Vector Machines (Radial Basis Function)	C = 1000	Internal External	92.1 94.2	94.8 97.1	89.7 91.6	0.92 0.94
Support Vector Machine (Polynomial Kernel)	C = 1000 Polynomial Degree = 2	Internal External	87.7 92.1	92.5 96.6	83.8 88.4	0.87 0.92
K-Nearest-Neighbors	Neighbors = 4 Distance Metric = Minkowski Weights = 'distance'	Internal External	93.1 90.9	94.0 93.6	92.3 88.6	0.93 0.91
AdaBoost	Num. Estimators = 200 Learning Rate = 1 Estimator = Decision Tree	Internal External	88.8 92.9	91.1 97.2	86.7 89.2	0.88 0.93
Histogram Gradient Boosting	Learning Rate = 0.1 Max Iterations = 100 Max Depth = None	Internal External	93.1 93.2	95.0 96.7	91.4 90.3	0.93 0.93
Bagging Estimators	Num. Estimators = 500	Internal External	93.3 93.8	94.3 96.0	92.4 91.9	0.93 0.94
Stacked Generalization	Estimator = Logistic Regression Cross Validation = 'prefit'	Internal External	94.3 92.9	94.8 94.9	93.8 91.0	0.94 0.93
Majority Voting Classifier	N/A	Internal External	92.6 93.3	95.9 96.9	89.9 90.3	0.92 0.93

Results - Fixing “Symmetry Traps”

- Accuracy: 91.9%
- Sensitivity: 0.674
- Specificity: 0.940

The distribution of ψ for correct and incorrect frames was measured.

- Average $\psi_{correct} = 16.6^\circ$.
- Average $\psi_{incorrect} = 7.12^\circ$.

Results - Stratified ψ Correction Performance

Table 2: Stratified ψ Test Set Stacked Generalization Classification Performance

Psi Range	Sample Size	Accuracy (%)	Sensitivity (%)	Specificity (%)	F1-Score
0 – 5°	488	71.0	71.4	70.7	0.69
5 – 10°	1132	88.2	90.5	86.0	0.88
10 – 15°	1224	93.0	92.8	93.2	0.93
15 – 20°	1107	96.1	97.0	95.3	0.96
> 20°	3568	98.3	98.3	98.2	0.98

Discussion

- Reliable post-processing method to overcome pernicious issue (30 years in the making!)
- Suggests an imaging setup for measuring kinematics slightly off-oblique to escape “ambiguous zone”

Background

Aims

Aim 1 - Joint Track Machine Learning

Aim 2 - Correcting Symmetric Implant Ambiguity

Aim 3 - Musings on a “Kinematics Translator” and Synthetic Kinematics Data

Aim 4 - This will definitely work on shoulders, right?

Conclusion

References

Background

Aims

Aim 1 - Joint Track Machine Learning

Aim 2 - Correcting Symmetric Implant Ambiguity

Aim 3 - Musings on a “Kinematics Translator” and Synthetic Kinematics Data

Aim 4 - This will definitely work on shoulders, right?

Conclusion

References

Spoiler Alert

No, it won't.



Goal

Establish a protocol for exploring the relative sensitivity of input orientation to projected shape

Table 1: Root mean squared differences between JointTrack Machine Learning optimized kinematics and manually registered kinematics on single-plane fluoroscopy

Implant Type	$x_{trans}(mm)$	$y_{trans}(mm)$	$z_{trans}(mm)$	$x_{rot}(\circ)$	$y_{rot}(\circ)$	$z_{rot}(\circ)$
Humeral	8.46	8.64	152.78	22.59	64.74	11.81
Glenosphere	0.97	1.44	32.58	13.72	26.40	8.30
Femoral	0.57	0.39	26.95	0.66	0.73	0.60
Tibial	0.67	0.64	27.17	1.63	2.74	0.66

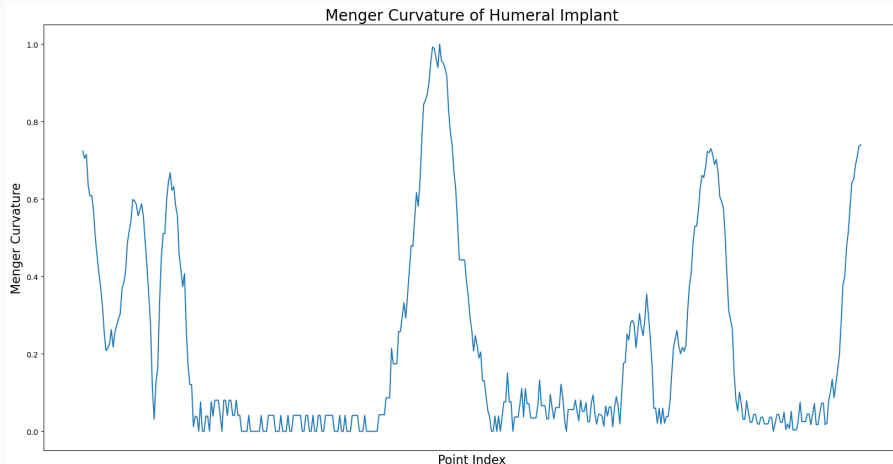
Modified Mean Surface Distance

- In order to improve error gradient, a modified mean surface distance was incorporated into the cost function.
- The mean of the dot product between the projection estimate and a distance map of the CNN segmentation.

$$J = \frac{\text{Proj} \cdot DM}{\sum \text{Proj}} \quad (1)$$

Modified Asymmetric Keypoint Distance

- Early psychological research deemed curvature as highly salient for object recognition [1, 2]. This aimed to place additional emphasis on autonomously selected high-curvature regions.
 - Extracted regions of high-curvature using Menger's Algorithm [25].



Modified Asymmetric Keypoint Distance

- Utilized a modified asymmetric surface distance on the discrete set of keypoints.

$$J = \frac{\sum_{k \in \mathbb{K}} (\min_{p \in \text{Proj}} (p \cdot DM_k))}{N_k}$$

where (2)

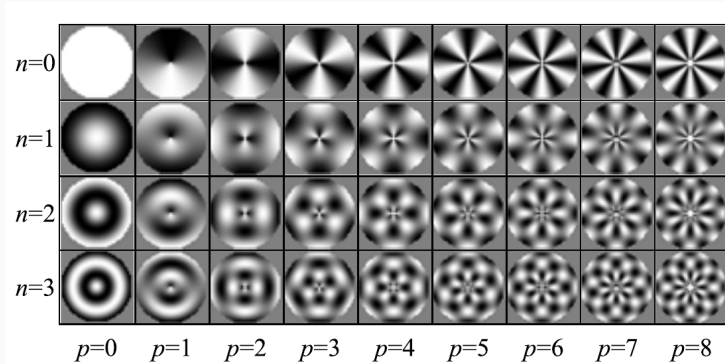
\mathbb{K} = Set of all keypoints

DM_k = Distance map for keypoint k

2-Dimensional Shape

Invariant Angular Radial Transform Descriptor

The Invariant Angular Radial Transform provides an orthogonal spatial basis function to describe binary images.



The basis “vectors” for the invariant angular radial transform. From [24].

IARTD Feature Vector

The complex feature vector for IARTD is constructed to ensure orthogonality and rotational invariance for the magnitude. Prior to calculation, the image coordinates are normalized such that $(0, 0)$ is at the center, and each of the four corners are $(\pm 1, \pm 1)$.

$$F_{np} = \int_0^{2\pi} \int_0^1 f(\rho, \theta) V_{np}(\rho, \theta) \rho d\rho d\theta \quad (3)$$

$f(\rho, \theta) \equiv$ Input image in polar coordinates

$$V_{np}(\rho, \theta) = \frac{1}{2\pi} e^{j p \theta} R_n(\rho) \quad (4)$$
$$R_n(\rho) = \begin{cases} 1 & n = 0 \\ 2 \cos(\pi n \rho) & n \neq 0 \end{cases}$$

Normalizing IARTD Feature Vector

We normalize the phase of the feature vector to ensure full rotational invariance.

$$\begin{aligned}\phi'_{np} &= \phi_{np} - \phi_{n,1} \\ F'_{np} &= F_{np} e^{-jp\phi_{n,1}}\end{aligned}\tag{5}$$

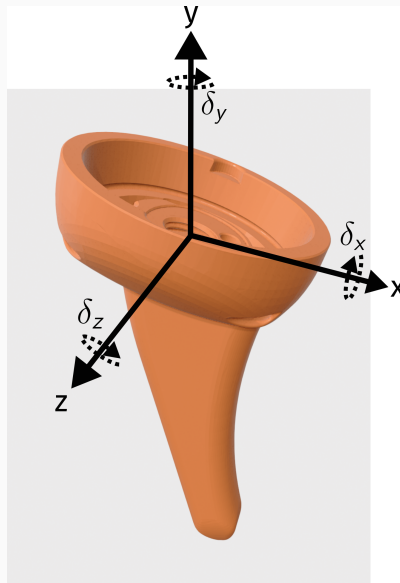
The final feature vector is constructed with the corrected phase and magnitude values. Values of $p < 2$ are redundant and removed per the original authors' suggestion [24].

$$IARTD = \{|F'_{np}|, \phi'_{np}\} \text{ where } n \geq 0, p \geq 2\tag{6}$$

Methods - Shape Difference

The “input shapes” for each implant were the projected implants at $\pm 30^\circ$ along each rotational axis at 5° increments. 1° perturbations were applied along each rotation axis.

$$\begin{aligned}\Delta S(\delta)_{z,x,y} \equiv & IARTD(R_{z,x,y,+\delta}) \\ & - IARTD(R_{z,x,y,-\delta}) \quad (7) \\ \forall \delta \in & \{\delta_x, \delta_y, \delta_z\}\end{aligned}$$



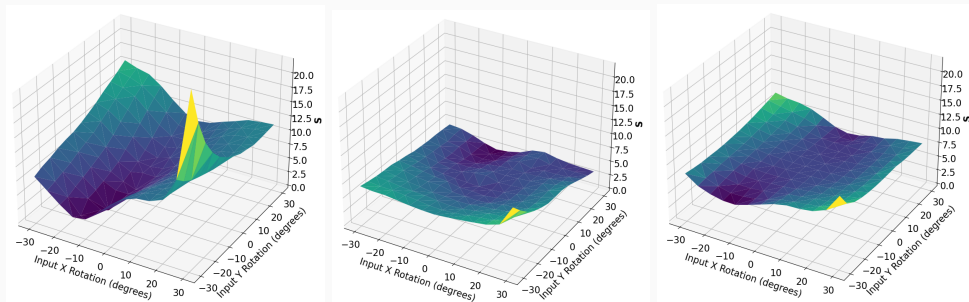
Methods - Shape Sensitivity

The $\Delta S(\delta)_{z,x,y}$ vector is normalized to account for overall scale of each element, in-plane rotation inputs are averaged, and the 2-norm of the difference vector is defined as the shape sensitivity.

A larger vector would indicate that the shape changed more for that particular “input shape” and perturbation.

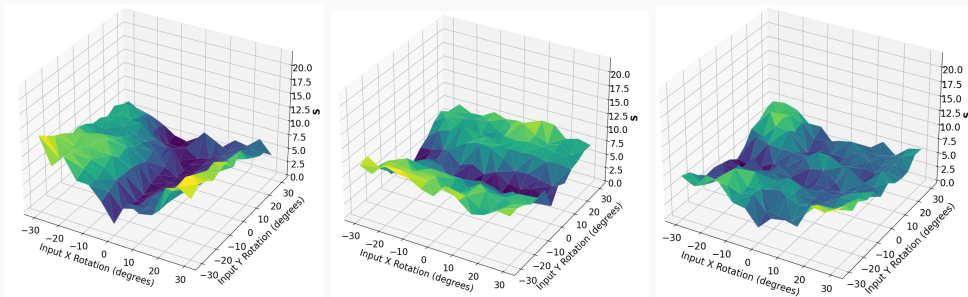
$$S(\delta)_{x,y} = \frac{\sum_z \|S(\delta)_{z,x,y}\|_2}{N} \quad (8)$$

Results - Humeral Shape Sensitivity



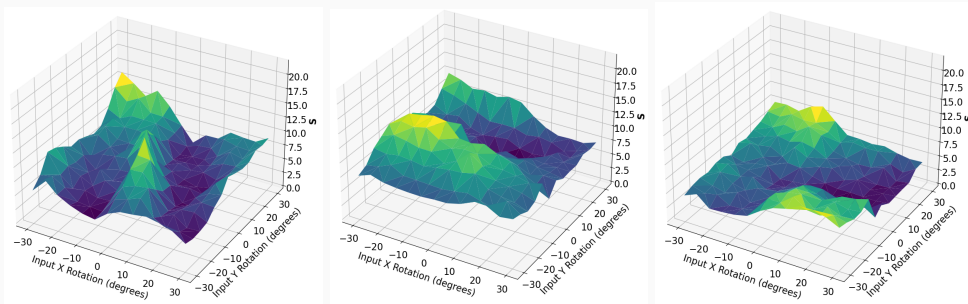
The \mathbb{S} plot for a humeral implant for δ rotations along the x, y, and z axis, respectively.

Results - Glenosphere Shape Sensitivity



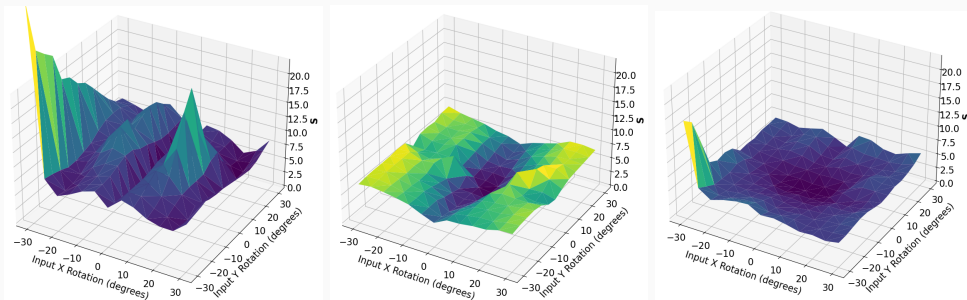
The $\$$ plot for a glenosphere implant for δ rotations along the x, y, and z axis, respectively.

Results - Femoral Shape Sensitivity



The $\$$ plot for a femoral implant for δ rotations along the x, y, and z axis, respectively.

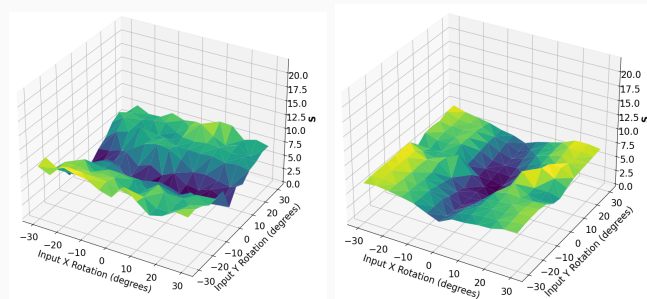
Results - Tibial Shape Sensitivity



The \mathbb{S} plot for a tibial implant for δ rotations along the x, y, and z axis, respectively.

Key Takeaways

- Humeral implant has the lowest δ_y sensitivity of all implants, which is the difficult registration axis.
- Tibial and glenosphere implants demonstrate a “valley” along rotation axis representing near-symmetry.
 - For tibial implants, this is the axis most commonly associated with “symmetry traps”.



Glenosphere (left) and tibial (right) δ_y shape sensitivities.

Conclusion

Conclusions

Throughout the past four years, I have:

1. Established a fully autonomous method of measuring TKA kinematics from single plane fluoroscopy. This software is used globally by different research groups, and offers
2. Utilized machine learning to address “symmetry traps”, an inherent limitation in single-plane TKA kinematics measurements for nearly 30 years. Additionally, we offer an alternative imaging protocol for accurately measuring TKA kinematics in a clinical setting.
3. Developed a pipeline for accessing the relative performance of autonomous registration for different implants, conclusively finding that implant geometry alone is not sufficient for every joint.

Presentations

- [1] Scott Banks, Andrew James Jensen, and Paris Flood. *In Regione Caecorum Rex Est Lucus - Towards Routine Clinical Examinations of Joint Kinematics.* Oslo, Norway, 2019.
- [2] Paris Flood, Andrew Jensen, and Scott Banks. *Towards Practical Clinical Examination of 3D Joint Kinematics Using Machine Learning.* Podium. Toronto, Ontario, 2019.
- [3] Andrew Jensen, Yifei Dai, and Andrea Gardner. *Impact of Sagittal Resection Variability on Implant Fit during Partial Knee Arthroplasty.* Podium. Phoenix, AZ, Feb. 2020.
- [4] Andrew Jensen et al. *Comparison of Clinical and Computational Implant Fit Analysis in Partial Knee Arthroplasty.* Podium. Phoenix, AZ, Feb. 2020.
- [5] Andrew Jensen et al. *Towards Routine Clinical Examination of 3D Joint Kinematics.* Korea, 2020.

Presentations ii

- [6] Yifei Dai et al. *Comparative Analysis of Fixation Structure Design on the Primary Stability of Cementless TKA during Walking.* Podium. Online, Feb. 2021.
- [7] Yifei Dai et al. *Impact of Fixation Components on Primary Stability of Cementless TKA during Walking.* Podium. Online, Feb. 2021.
- [8] Andrew Jensen et al. *Accuracy of an Autonomous Method for Extracting Joint Kinematics from Single-Plane Fluoroscopy.* Oslo, Norway, 2021.
- [9] Andrew James Jensen et al. *An Autonomous Method for Extracting 3D Knee Replacement Kinematics from Dynamic Single Plane Fluoroscopic Images.* Online, 2021.
- [10] Jacob Griffith et al. *Automated Segmentation and Grading of Rodent Knee OA Histology Using Convolutional Neural Networks.* Poster. Tampa, FL, Feb. 2022.
- [11] Andrew Jensen, Lindsey Palm, and Scott Banks. *Autonomous Measurement of 3D TKA Kinematics from Dynamic Single-Plane Fluoroscopic Images.* Podium. Tampa, FL, Feb. 2022.
- [12] Andrew Jensen. *Deep Learning for Image Processing in Orthopaedics.* Virtual Scientific Session. Online, Jan. 2023.

Presentations iii

- [13] Andrew J. Jensen et al. *Overcoming Single-Plane Limitations in TKA Kinematics Measurements Using Machine Learning*. Podium. New York, NY, Sept. 2023.

Publications

- [1] William Burton et al. “Automatic Tracking of Healthy Joint Kinematics from Stereo-Radiography Sequences.”. In: *Computers in Biology and Medicine* (2021). DOI: 10.1016/j.combiomed.2021.104945.
- [2] Jordan S. Broberg et al. “Validation of a Machine Learning Technique for Segmentation and Pose Estimation in Single Plane Fluoroscopy”. In: *Journal of Orthopaedic Research* (Feb. 2023). ISSN: 0736-0266, 1554-527X. DOI: 10.1002/jor.25518. (Visited on 02/13/2023).
- [3] Andrew J. Jensen et al. “Joint Track Machine Learning: An Autonomous Method of Measuring Total Knee Arthroplasty Kinematics From Single-Plane X-Ray Images”. In: *The Journal of Arthroplasty* 38:10 (May 2023), pp. 2068–2074. ISSN: 08835403. DOI: 10.1016/j.arth.2023.05.029. (Visited on 06/22/2023).

Timeline

Date(s)	Event
2015-2019	Mech. Eng. B.S, Magna Cum Laude, UF
April 2019 - April 2020	Internship at Exactech
April 2020	Started in Miller Lab
August 2020	Officially Started PhD at UF
November 2021	Best Presentation Award at ISTA: Emerging Technologies
April 2022	Submitted JTM for HAP Paul Award
September 2022	HAP Paul Award at ISTA 2022
November 2023	Symmetry Trap Paper Submitted
December 2023	Part-time Internship at Exactech Started
February 2024	Revisions Requested for Symmetry Trap Paper
February 2024	Implant Shape Sensitivity Paper Submitted
March 2024	Revised Symmetry Trap Paper Submitted

Thank you!

Thanks for listening!!

References

References

- [1] Fred Attneave. “**Some Informational Aspects of Visual Perception.**”. In: *Psychological Review* 61.3 (1954), pp. 183–193. ISSN: 1939-1471, 0033-295X. DOI: 10.1037/h0054663. (Visited on 11/02/2023).
- [2] Fred Attneave and Malcolm D. Arnoult. “**The Quantitative Study of Shape and Pattern Perception.**”. In: *Psychological Bulletin* 53.6 (Nov. 1956), pp. 452–471. ISSN: 1939-1455, 0033-2909. DOI: 10.1037/h0044049. (Visited on 11/02/2023).
- [3] Charles Audet and Warren Hare. ***Derivative-Free and Blackbox Optimization.*** Springer Series in Operations Research and Financial Engineering. Cham: Springer International Publishing, 2017. ISBN: 978-3-319-68912-8 978-3-319-68913-5. DOI: 10.1007/978-3-319-68913-5. (Visited on 01/27/2023).
- [4] Ishan Bajaj, Akhil Arora, and M. M. Faruque Hasan. “**Black-Box Optimization: Methods and Applications.**”. In: (Jan. 2021), pp. 35–65. DOI: 10.1007/978-3-030-66515-9_2.

References ii

- [5] P. N. Baker et al. “The Role of Pain and Function in Determining Patient Satisfaction After Total Knee Replacement: Data From the National Joint Registry for England and Wales”. In: *The Journal of Bone and Joint Surgery. British volume* 89-B.7 (July 2007), pp. 893–900. ISSN: 0301-620X, 2044-5377. DOI: 10.1302/0301-620X.89B7.19091. (Visited on 03/22/2021).
- [6] S.A. Banks and W.A. Hodge. “Accurate Measurement of Three-Dimensional Knee Replacement Kinematics Using Single-Plane Fluoroscopy”. In: *IEEE Transactions on Biomedical Engineering* 43.6 (June 1996), pp. 638–649. ISSN: 00189294. DOI: 10.1109/10.495283. (Visited on 03/22/2021).
- [7] C. Bradford Barber, David P. Dobkin, and Hannu Huhdanpaa. “The Quickhull Algorithm for Convex Hulls”. In: *ACM Transactions on Mathematical Software* 22.4 (Dec. 1996), pp. 469–483. ISSN: 0098-3500, 1557-7295. DOI: 10.1145/235815.235821. (Visited on 02/20/2023).
- [8] Robert B. Bourne et al. “Patient Satisfaction after Total Knee Arthroplasty: Who Is Satisfied and Who Is Not?” In: *Clinical Orthopaedics & Related Research* 468.1 (Jan. 2010), pp. 57–63. ISSN: 0009-921X. DOI: 10.1007/s11999-009-1119-9. (Visited on 03/22/2021).

References iii

- [9] Jordan S. Broberg et al. “Validation of a Machine Learning Technique for Segmentation and Pose Estimation in Single Plane Fluoroscopy”. In: *Journal of Orthopaedic Research* (Feb. 2023). ISSN: 0736-0266, 1554-527X. DOI: 10.1002/jor.25518. (Visited on 02/13/2023).
- [10] William Burton et al. “Automatic Tracking of Healthy Joint Kinematics from Stereo-Radiography Sequences.”. In: *Computers in Biology and Medicine* (2021). DOI: 10.1016/j.combiomed.2021.104945.
- [11] Alexander Buslaev et al. “Albumentations: Fast and Flexible Image Augmentations”. In: *Information* 11.2 (Feb. 2020), p. 125. ISSN: 2078-2489. DOI: 10.3390/info11020125. (Visited on 10/24/2020).
- [12] T. M. Chan. “Optimal Output-Sensitive Convex Hull Algorithms in Two and Three Dimensions”. In: *Discrete & Computational Geometry* 16.4 (Apr. 1996), pp. 361–368. ISSN: 0179-5376, 1432-0444. DOI: 10.1007/BF02712873. (Visited on 02/20/2023).

- [13] P. D. L. Flood and Scott A. Banks. “Automated Registration of 3-D Knee Implant Models to Fluoroscopic Images Using Lipschitzian Optimization”. In: *IEEE Transactions on Medical Imaging* 37.1 (2018), pp. 326–335. DOI: [10.1109/tmi.2017.2773398](https://doi.org/10.1109/tmi.2017.2773398).
- [14] Bo Gao and Naiquan (Nigel) Zheng. “Investigation of Soft Tissue Movement during Level Walking: Translations and Rotations of Skin Markers”. In: *Journal of Biomechanics* 41.15 (Nov. 2008), pp. 3189–3195. ISSN: 00219290. DOI: [10.1016/j.jbiomech.2008.08.028](https://doi.org/10.1016/j.jbiomech.2008.08.028). (Visited on 03/31/2022).
- [15] R.L. Graham. “An Efficient Algorithm for Determining the Convex Hull of a Finite Planar Set”. In: *Information Processing Letters* 1.4 (June 1972), pp. 132–133. ISSN: 00200190. DOI: [10.1016/0020-0190\(72\)90045-2](https://doi.org/10.1016/0020-0190(72)90045-2). (Visited on 02/20/2023).
- [16] John C. Ivester et al. “A Reconfigurable High-Speed Stereo-Radiography System for Sub-Millimeter Measurement of In Vivo Joint Kinematics”. In: *Journal of Medical Devices* 9.4 (Dec. 2015), p. 041009. ISSN: 1932-6181, 1932-619X. DOI: [10.1115/1.4030778](https://doi.org/10.1115/1.4030778). (Visited on 10/18/2022).
- [17] R A Jarvis. “On the Identification of the Convex Hull of a Finite Set of Points in the Plane”. In: (1973).

- [18] Andrew J. Jensen et al. “**Joint Track Machine Learning: An Autonomous Method of Measuring Total Knee Arthroplasty Kinematics From Single-Plane X-Ray Images**”. In: *The Journal of Arthroplasty* 38.10 (May 2023), pp. 2068–2074. ISSN: 08835403. DOI: 10.1016/j.arth.2023.05.029. (Visited on 06/22/2023).
- [19] B L Kaptein et al. “**Evaluation of Three Pose Estimation Algorithms for Model-Based Roentgen Stereophotogrammetric Analysis**”. In: *Proceedings of the Institution of Mechanical Engineers, Part H: Journal of Engineering in Medicine* 218.4 (Apr. 2004), pp. 231–238. ISSN: 0954-4119, 2041-3033. DOI: 10.1243/0954411041561036. (Visited on 12/19/2022).
- [20] Mei-Ying Kuo et al. “**Influence of Soft Tissue Artifacts on the Calculated Kinematics and Kinetics of Total Knee Replacements during Sit-to-Stand**”. In: *Gait & Posture* 33.3 (Mar. 2011), pp. 379–384. ISSN: 09666362. DOI: 10.1016/j.gaitpost.2010.12.007. (Visited on 09/09/2021).
- [21] Steven Kurtz et al. “**Projections of Primary and Revision Hip and Knee Arthroplasty in the United States from 2005 to 2030:**” in: *The Journal of Bone & Joint Surgery* 89.4 (Apr. 2007), pp. 780–785. ISSN: 0021-9355. DOI: 10.2106/JBJS.F.00222. (Visited on 01/20/2021).

- [22] Mario A. Lafortune et al. “**Three-Dimensional Kinematics of the Human Knee during Walking**”. In: *Journal of Biomechanics* (1992). DOI: 10.1016/0021-9290(92)90254-x.
- [23] S. Lavallee and R. Szeliski. “**Recovering the Position and Orientation of Free-Form Objects from Image Contours Using 3D Distance Maps**”. In: *IEEE Transactions on Pattern Analysis and Machine Intelligence* 17.4 (Apr. 1995), pp. 378–390. ISSN: 01628828. DOI: 10.1109/34.385980. (Visited on 05/12/2021).
- [24] Jong-Min Lee and Whoi-Yul Kim. “**A New Shape Description Method Using Angular Radial Transform**”. In: *IEICE Transactions on Information and Systems* E95.D.6 (2012), pp. 1628–1635. ISSN: 0916-8532, 1745-1361. DOI: 10.1587/transinf.E95.D.1628. (Visited on 11/21/2023).
- [25] J. C. Léger. **Menger Curvature and Rectifiability**. Apr. 1999. arXiv: math/9905212. (Visited on 01/10/2024).
- [26] Cheng-Chung Lin et al. “**Effects of Soft Tissue Artifacts on Differentiating Kinematic Differences between Natural and Replaced Knee Joints during Functional Activity**”. In: *Gait & Posture* 46 (May 2016), pp. 154–160. ISSN: 09666362. DOI: 10.1016/j.gaitpost.2016.03.006. (Visited on 09/09/2021).

References vii

- [27] M.R. Mahfouz et al. “A Robust Method for Registration of Three-Dimensional Knee Implant Models to Two-Dimensional Fluoroscopy Images”. In: *IEEE Transactions on Medical Imaging* 22.12 (Dec. 2003), pp. 1561–1574. ISSN: 0278-0062. DOI: 10.1109/TMI.2003.820027. (Visited on 03/22/2021).
- [28] Tuuli Saari et al. “Knee Kinematics in Medial Arthroscopy. Dynamic Radiostereometry during Active Extension and Weight-Bearing”. In: *Journal of Biomechanics* 38.2 (Feb. 2005), pp. 285–292. ISSN: 00219290. DOI: 10.1016/j.jbiomech.2004.02.009. (Visited on 09/09/2021).
- [29] C. E. H. Scott et al. “Predicting Dissatisfaction Following Total Knee Replacement: A Prospective Study of 1217 Patients”. In: *The Journal of Bone and Joint Surgery. British volume* 92-B.9 (Sept. 2010), pp. 1253–1258. ISSN: 0301-620X, 2044-5377. DOI: 10.1302/0301-620X.92B9.24394. (Visited on 03/22/2021).
- [30] Göran Selvik. “Roentgen Stereophotogrammetry: A Method for the Study of the Kinematics of the Skeletal System”. In: *Acta Orthopaedica Scandinavica* 60.sup232 (Jan. 1989), pp. 1–51. ISSN: 0001-6470. DOI: 10.3109/17453678909154184. (Visited on 02/14/2023).

References viii

- [31] Bruno O. Shubert. “A Sequential Method Seeking the Global Maximum of a Function”. In: *SIAM Journal on Numerical Analysis* 9.3 (1972), pp. 379–388. DOI: 10.1137/0709036. eprint: <https://doi.org/10.1137/0709036>.
- [32] Henri A Vrooman et al. “Fast and Accurate Automated Measurements in Digitized Stereophotogrammetric Radiographs”. In: *Journal of Biomechanics* 31.5 (May 1998), pp. 491–498. ISSN: 00219290. DOI: 10.1016/S0021-9290(98)00025-6. (Visited on 09/09/2021).
- [33] Jingdong Wang et al. “Deep High-Resolution Representation Learning for Visual Recognition”. In: *arXiv:1908.07919 [cs]* (Mar. 2020). arXiv: 1908.07919 [cs]. (Visited on 09/29/2020).
- [34] S. Zuffi et al. “A Model-Based Method for the Reconstruction of Total Knee Replacement Kinematics”. In: *IEEE Transactions on Medical Imaging* 18.10 (Oct./1999), pp. 981–991. ISSN: 02780062. DOI: 10.1109/42.811310. (Visited on 09/01/2020).